LEGIBILITY NOTICE

A major purpose of the Technical Information Center is to provide the broadest dissemination possible of information contained in DOE's Research and Development Reports to business, industry, the academic community, and federal, state and local governments.

Although a small portion of this report is not reproducible, it is being made available to expedite the availability of information on the research discussed herein.

LA-UR -89-2187

LA-UR--89-2187

DE89 014277

Los Alamos National Laboratory is operated by the University of California for the United States Department of Energy under contract W-7405-ENG-36

TITLE INSTABILITY OF CONCAVE CONDUCTOR SURFACES AT HIGH MAGNETIC PRESSURE

AUTHOR(S) J. V. Parker, P-DO
R. L. Bowers, X-10
M. G. Sheppard, X-10
D. L. Weiss, X-10

SUBMITTED TO Fifth International Conference on Megagauss Magnetic Field Generation and Related Topics, Novosibirsk, USSR
July 3-7, 1989

DISCLAIMER

MASTER

Los Alamos Los Alamos National Laboratory
Los Alamos, New Mexico 87545

FORM NO. 836 R4

INSTABILITY OF CONCAVE CONDUCTOR SURFACES AT HIGH MAGNETIC PRESSURE

J. V. Parker, R. L. Bowers, M. G. Sheppard, and D. L. Weiss

Los Alamos National Laboratory, Los Alamos, New Mexico 87545

I. INTRODUCTION

At magnetic fields in excess of a few 100 T the energy dissipation in a conductor surface exceeds the characteristic vaporization energy and the metal conductor is disrupted. The threshold for this process, termed an "electrical explosion" by Demichev and Shneerson [1], is usually considered to be the field where the magnetic energy density $B_S^2/2\mu_0$ is equal to the volumetric evaporation energy density, Q_S. However, Q_S is not a uniquely defined quantity. Physically, "evaporation" is understood to mean a sufficient reduction in the average density of the conductor so that the resistivity rises to a high value and current flow is reduced. This reduction in density is opposed by the applied magnetic pressure and by the inertia of the material and thus Q_S is a function of both B_S and time. The definition of B_S is, therefore, an implicit one, $B_S = (2\mu Q_S[B_S Kt])^{1/2}$, and prediction of the "electrical explosion" requires a 1-D or 2-D MHD calculation using the complete mechanical and electrical equation of state (EOS) for the conductor material.

Such a calculation can be carried out with reasonable accuracy over the pressure and temperature range where the EOS is known from laboratory measurements. At the temperatures and pressures of interest in many high magnetic field experiments the EOS is not available from laboratory measurements and must be taken from theoretical models [2,3]. Generally, there are a number of different equations of state, even for well studied materials such as copper, and the differences among these EOS models may produce strikingly different numerical predictions of the conductor response at high magnetic field.

We have begun a series of experiments at Los Alamos with the purpose of providing data on conductor response at high magnetic field. These experiments are closely linked to a numerical modeling effort that uses the experimental data to refine the high pressure/high temperature EOS of the conductor materials studied.

This paper describes the results of the first experiment in this series and the analysis of the results obtained. The experiment was only partially successful in obtaining the conductor response data sought. During the experiment, an unexpectedly strong instability was observed that we believe may be an important cause of failure in high magnetic field apparatus.

Section II of the paper describes the experimental apparatus and diagnostics. Section III discusses predictions of the conductor response based on both 1-D and 2-D magneto-hydrodynamic calculations. The experimental results are summarized in Section IV with particular regard to the surface instability observed. Analysis of the experimental results is presented in Section V followed by a brief summary of our conclusions in Section VI.

II. DESCRIPTION OF THE EXPERIMENT

The experimental sample is in the form of a cylindrical rod located on the axis of a coaxial conductor system. This geometry provides a uniform surface current in the sample, free of edge effects, and places the sample in uniform compression so there is no net acceleration of the sample. This geometry is similar to that employed by Spielman, Hussey, and Lopez [4] in their experiments but we employ a larger sample, and a longer pulse duration to facilitate measurements on the conductor.

The experimental sample is shown in Fig. 1. The upper half of Fig. 1 shows the preliminary sample design. Measurements are performed on the central region which is 1.0 cm in diameter and 1.9 cm in length. In the preliminary design the ends of the central section flare at a 20° angle to a diameter of 2 cm and then merge into the heavy end sections. Electrical connection is made to the end region at a radius of 4 cm to reduce contact arcing.

The lower half of Fig. 1 shows the final sample design in which the 20° flare has been replaced with a circular arc of radius 1.59 cm. the reason for this design change is discussed in Section III. the sample was machined from a solid piece of OFHC copper on a numerically controlled lathe. Great care was taken to make the circular arc tangent to the surface of the central rod.

One of the primary objectives of the experiment is to measure the rate of current penetration into the sample. This is accomplished by boring a hole through the center of the sample and inserting an insulated conductor as shown in Fig. 1. During the experiment, current flows first on the outside surface of the copper rod. After an interval of several microseconds, the current diffuses to the inner surface of the copper where it creates an electric field equal to $\epsilon = \delta j(t)$, where δ is the copper resistivity. The central rod is connected to the sample at the bottom and a voltage $V(t) = \delta j(t)\ell_{*c}$, where ℓ_{*c} is the effective length of the central region, appears between the top end of the rod and the sample. The measured signal $V(t)$ can be compared directly with the predictions of an MHD calculation. while this is not a direct measurement of the resistivity, an extensive set of measurements with different sample thicknesses and peak currents will provide ample data to test the validity of EOS models.

For the first experiment, the central rod was 6061-T6 aluminum. The surface was anodized to a thickness of 0.064 mm to provide electrical insulation.

The experiment is performed with the sample mounted in a reusable experimental chamber as shown in Fig. 2. To reduce electrical noise, the sample voltage is measured by connecting a resistor across the terminals and measuring the current with a Pearson Electronics Model 411 Current Transformer.

In addition to the sample voltage, several other diagnostics were employed on the experiment. Current was measured at two locations using the Faraday rotation of a HeNe laser beam in a glass fiber. An array of five magnetic probe loops were positioned along a radius starting at r = 2.5 cm in steps of 2.5 cm to check for electrical breakdown in the vacuum region.

III. MAGNETOHYDRODYNAMIC SIMULATIONS

A series of magnetohydrodynamic simulations have been performed to investigate the behavior of large currents on the central rod shown in Fig. 1. A one-dimensional (1-D) implicit Lagrangian code has been used to model the behavior of the central portion of the rod, and a two-dimensional (2-D) Eulerian code has been used to model the current penetration near the ends. The codes used the same tabular equations of state and electrical resistivity for copper. The region outside of the copper was treated as a true vacuum in the 1-D simulations. In the 2-D simulations it was modeled as a low density gas of high resistivity to simulate a magnetic vacuum. Both sets of calculations used the same capacitor bank current drive, which was expected to consist of a 5.0 μs half cycle pulse peaking at 6.0 MA.

The radial profiles of density and magnetic field predicted by the 1-D code and by the 2-D code in the central region of the rod agreed quite well. The rate of current penetration into the central portion of the rod is shown in Fig. 3. The 1-D calculations predict that the electric current will reach the central insulator at r = 0.4 cm about 3.5 μs into the experiment.

The initial setup for the 2-D calculations represent the left half of the rod, including the left-hand electrode wall. The initial design consisted of a beveled portion of copper connecting the electrode wall to the central rod (upper half of Fig. 1.). Figure 4 shows the region of the rod where the central rod joins the bevel at t = 3.7 μs. Figure 4a shows iso-density contours (separated by intervals of 1.0 g/cm^{-3}) and material velocity vectors, and Fig. 4b shows contours of rB_θ (separated by intervals of 0.1 MG-cm). Figure 4c shows contours of $log\ \eta$ where η is the electrical resistivity in $m\Omega$-cm. The current in the model at this time is about 5 MA. It will be noted that the current has penetrated further near the instability at z = 0.95 cm than in the regions further to the right. In fact, the perturbation is growing rapidly, eventually shearing the rod at the bevel.

The point at which the bevel joins the central rod represents a perturbation (corresponding to an ensemble of wavelengths) at the vacuum-copper interface. Since the magnetic Lorentz force associated with the current acts normal to the surface, the copper is accelerated in such a way as to produce a region of reduced density at this point. As the density drops, Joule heating melts the copper. The resistivity in the liquid regime increases rapidly with decreasing density, and the magnetic field diffuses further here than at other points along the rod or the bevel. Increased field penetration produces further heating and the process continues. It may be further noted that this is a regime where the fluid is unstable to magnetic Rayleigh-Taylor modes. The magnetic acceleration (in centimeters/microseconds) is of order

$$\alpha \approx \frac{I^2}{\pi r^2 \rho \ell_B} \quad .$$

where the current I is in units of 10^7 MA, the density is in g/cm^3, the radius in centimeters, and ℓ_b represents the magnetic field diffusion scale length. The corresponding linear growth time (in microseconds) for a perturbation of wavelength λ is

$$\tau \approx (\lambda/2\pi\alpha)^{1/2} \approx (1/2)\ell^{-1}$$

The magnetic scale length is about 0.08 cm (see Fig. 4b), so $\tau \approx 0.6\ \lambda^{1/2}$ for a current of 5 MA. The wave lengths which are expected to grown most rapidly are $\lambda \approx \ell_B \approx 0.08$ cm, for which $\tau \approx 0.16\ \mu$s.

The results of the 2-D calculations suggested that the bevel joining the rod to the electrode wall be replaced with a smoother contour, in this case a circle which is tangent to the rod, as shown in the lower half of Fig. 1. the point of tangency also represents a perturbation, but of a less severe nature. The results of 2-D simulations of this configuration indicated that the perturbations should not grow significantly during the first 4.0 μs when the current penetrated 0.1 cm into the rod. However, by about 7 μs three perturbations appeared with wave lengths of about 0.1 cm as shown by the isodensity contours in Fig. 5a. The spikes have saturated by this time, and are no longer growing. Figure 5b shows contours of constant rB_θ at intervals of 0.1 MG-cm.

IV. EXPERIMENTAL RESULTS

The experiment was performed at a bank charge voltage of 80 kV. The current waveform, derived from both the Faraday rotation and magnetic probe diagnostics, is shown in Fig. 6. The peak current of 3.9 MA corresponds to a peak magnetic field of 156 T and a peak pressure of 9.7 GPa (97 kbar). The risetime of the current pulse (3.5 μs) is longer than the time for a pressure wave to travel through the rod ($\sim$1.2 μs) so shock waves are not generated in the sample.

The current penetration measurement failed to produce any signal. We conjecture that the thin anodized insulation layer was disrupted by the applied pressure and shorted out the measuring circuit before current reached the inside surface of the sample. For future experiments we will consider using a thick-walled ceramic tube in place of the thin anodized layer.

The flash x-ray image shown in Fig. 7 provided the most interesting results of the experiment. Comparing the image on the right with the reference image on the left, taken before the experiment, one sees that deep grooves have been cut into the sample at both ends, starting almost exactly at the point where the straight cylinder blends into the 1.56 cm radius. Figure 8 gives a contour of the film density that shows more clearly the "spiky" nature of the low density regions which have cut into the sample. The average wavelength of this pattern is 0.85 mm. At least some of the material missing from the sample is ejected radially outward at a modest velocity. the signal on the closest magnetic

probe (~2 cm away) shows the influence of an expanding cloud of material at ~13 μs so the expansion velocity is 3–5 mm/μs.

At the time the x-ray image was exposed (~8.3 μs) the low density regions had penetrated through the copper and into the aluminum rod, a total depth of 2.6 mm. Without a second image, it is not possible to determine a growth rate but the depth is in reasonable agreement with the predictions of the 2-D MHD calculation discussed in Section III.

A microdensitometer scan across the constant diameter region of the sample shows that there is a small density increase on the sample surface consistent with the density decrease calculated with the 1-D MHD code.

V. ANALYSIS OF EXPERIMENT

Since the experiment did not deliver the expected current to the load, a series of 1-D simulations were performed using the observed current drive as shown in Fig. 6. These simulations included the AL_2O_3 ir 'ator at $r = 0.4$ cm. Profiles of mass density at several times are shown in Fig. 8a at five times into the current drive. Figure 8b shows profiles of rB_θ at the same times, and Fig. 8c shows the material temperature at these times.

VI. CONCLUSIONS

An instability has been observed in a cylindrical copper conductor at a megagauss magnetic field level. The instability causes thin finger-like regions of low material density to cut into the conductor surface. This instability resembles the classic "spike and bubble" of a Rayleigh-Taylor, but it is observed only in a region where the conductor has a convex surface. The adjacent straight section, subject to equal or greater magnetic field, is unaffected by this instability.

Simulations of the experiment performed with a 2-D MHD code and the SESAME equation of state predict an instability on the convex surface with a wavelength and growth rate similar to those observed experimentally. Examination of the numerical solution suggests that the instability has the following characteristics:

- The instability occurs when the surface of the conductor reaches a density and temperature where the variation of resistivity with density is very rapid.
- The concave surface is important because the magnetic pressure, acting normal to the surface, generates a tension force on a concave surface.
- The wavelength with maximum growth rate is related to the current penetration depth at the time the instability begins to grow

Further experimental investigations of this instability are planned to measure the growth rate and to investigate the effect of variations in geometry and material. Further calculations will be needed to clarify the importance of the resistivity EOS in the initiation and growth of the instability.

REFERENCES

1. V. F. Demichev and G. A. Shneerson, "Megagauss Magnetic Field Production by the Capacitor Bank Discharge," in Megagauss Technology and Pulsed Power Applications, Plenum Press, New York, 1987.

2. T. J. Burgess, "Electrical Resistivity Model of Metals," in Megagauss Technology and Pulsed Power Applications, Plenum Press, New York, 1987.

3. A. C. Mitchell and R. N. Keeler, "The Electrical Conductivity of copper and Aluminum at High Temperature and Pressure," in Megagauss Technology and Pulsed Power Applications, Plenum Press, New York, 1987.

4. R. B. Spielman, T. W. Hussey, and S. F. Lopez, "Megagauss Magnetic Field Generation on Proto-II," in Megagauss Technology and Pulsed Power Applications, Plenum Press, New York, 1987.

Figure Captions

Fig. 1. Experimental sample showing central anodized aluminum conductor for field penetration measurement.

Fig. 2. Experimental sample as mounted for experiment. Magnetic field diagnostic are positioned as shown.

Fig. 3. Radius (in cm) of significant current penetration into copper rod versus time (in μs) predicted for 5 μs half cycle, 6 MA drive.

Fig. 4 (a) Iso-density contours (in intervals of 1.0 g/cm^3) and material velocity vectors at 3.67 μs. The inner most contour represent a density of 10 g/cm^3; (b) Contours of constant rB_θ (in intervals of 0.1 MG-cm)s. The inner most contour corresponds to 0.1 MG-cm; (c) Contours of constant $log\ \eta$ (the intervals correspond to units of 0.8 and the resistivity is in mΩ-cm) at 3.67 μs. The inner most contour corresponds to $log\ \eta = -2.0$. Note the rapid transition to the resistivity used for the vacuum, $\eta = 10^{10}$ $m\Omega$-cm, and the high resistivity in the notch.

Fig. 5 (a) Iso-density contours (in intervals of 1.0 g/cm^3) at 7.0 μs for the geometry shown in the lower half of Fig. 1. The inner most contour represents a density of 10 g/cm^3; (b) Contours of constant rB_θ (in intervals of 0.1 MG-cm) at 7.0 μs. The inner most contour corresponds to 0.1 MG-cm.

Fig. 6 Current measurements from magnetic probes and Faraday rotation. Time of flash x-ray exposure is shown.

Fig. 7 Flash x-ray of sample. Left image taken prior to experiment. Right image at 8.3 μs shows well-developed instability at both concave regions.

Fig. 8 Constant density contour from flash x-ray showing spike-like structure of instability with a wavelength of $\sim$0.85 mm.

Fig. 9 (a) Mass density profiles, (b) profiles of rB_θ and (c) material temperature profiles at times in μs shown next to each curve from 1-D simulations using the observed current drive.

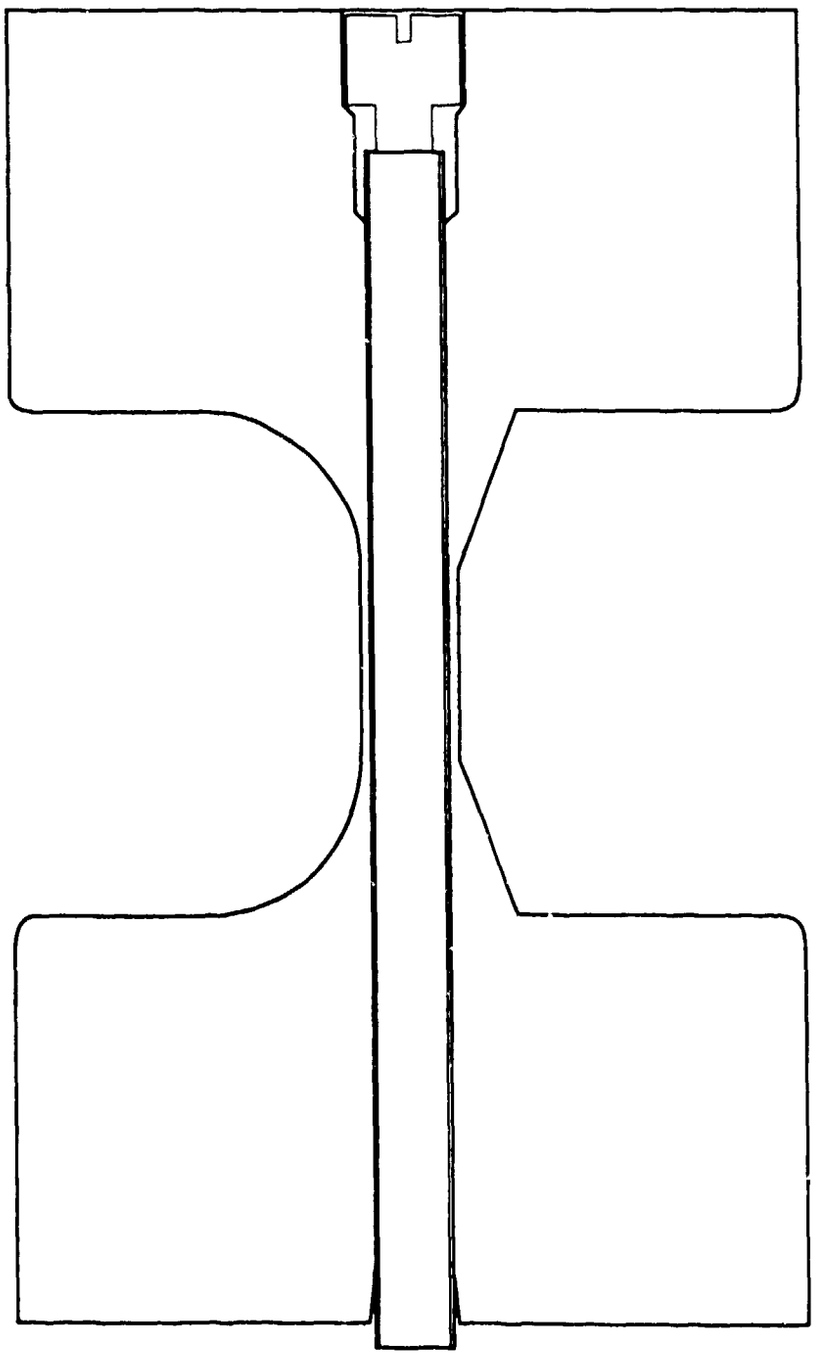

Fig 1

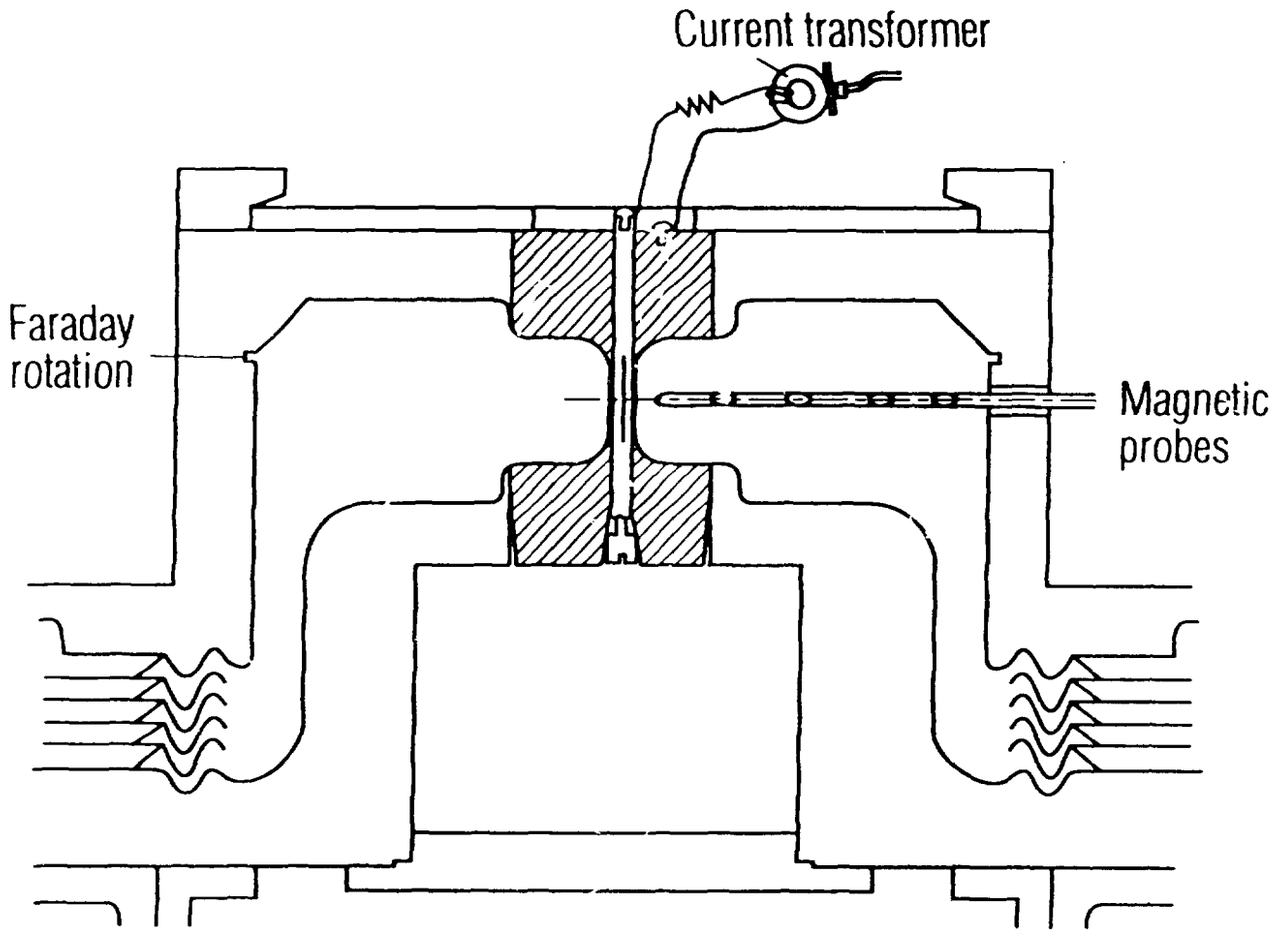

Fig. 2

Bowers fig 3

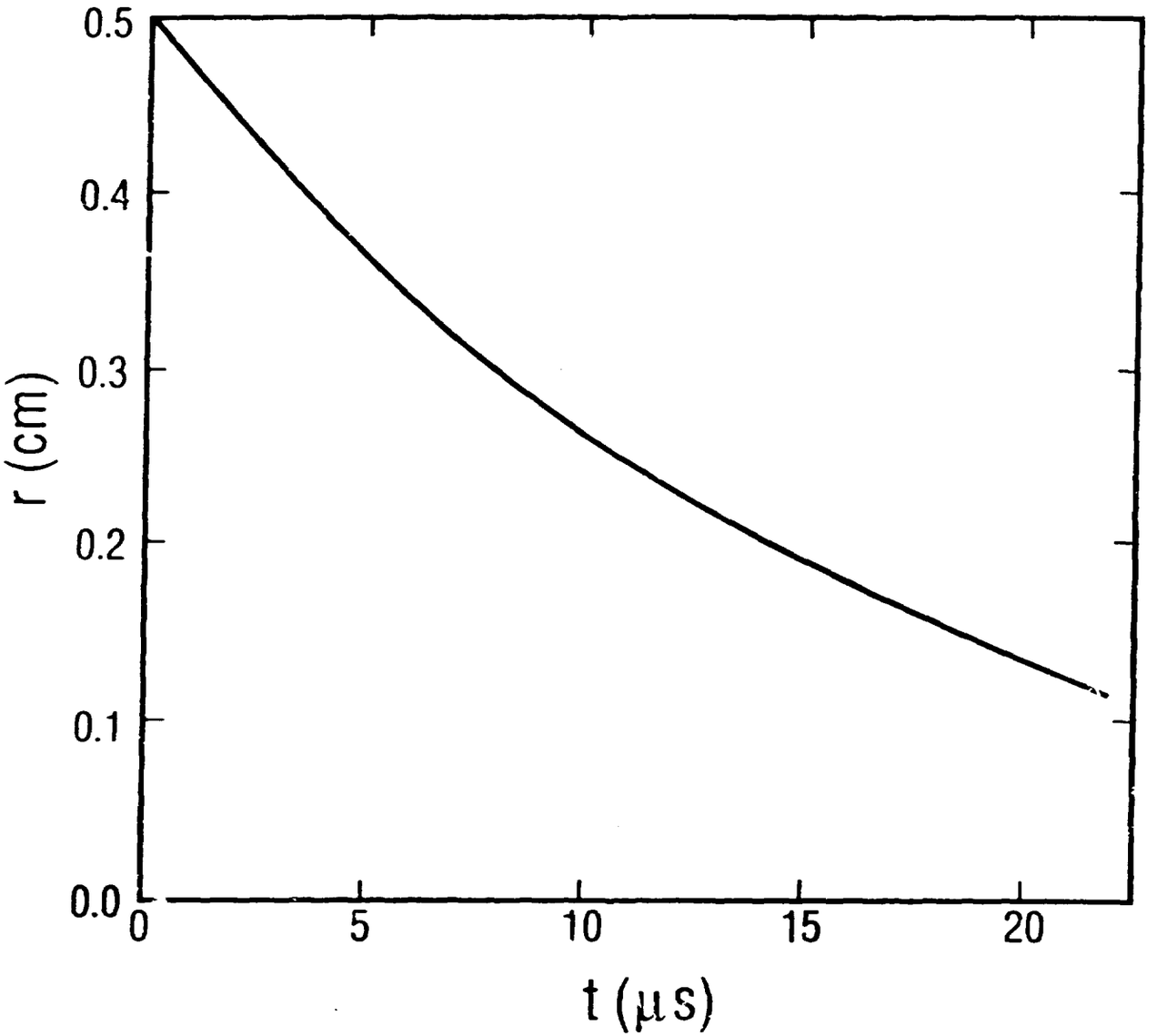

Fig. 3

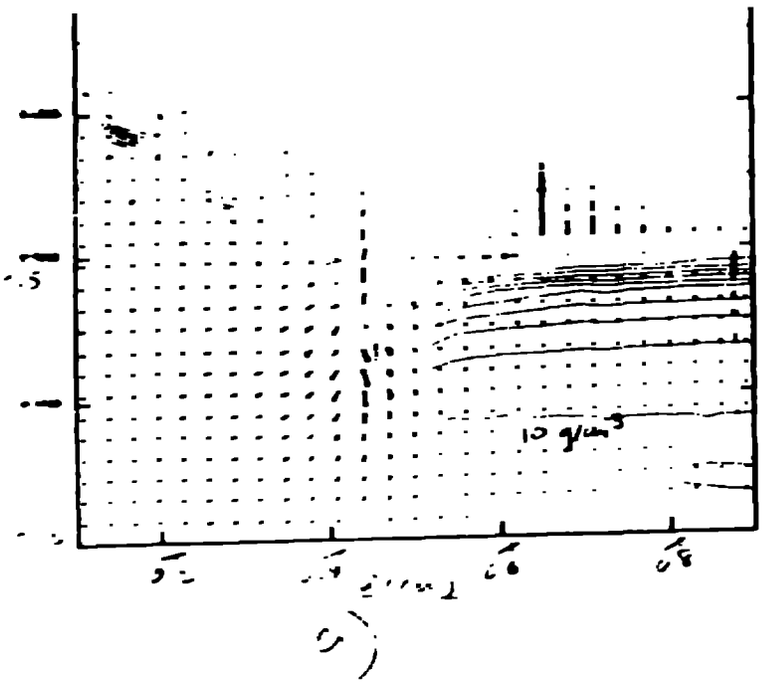

a)

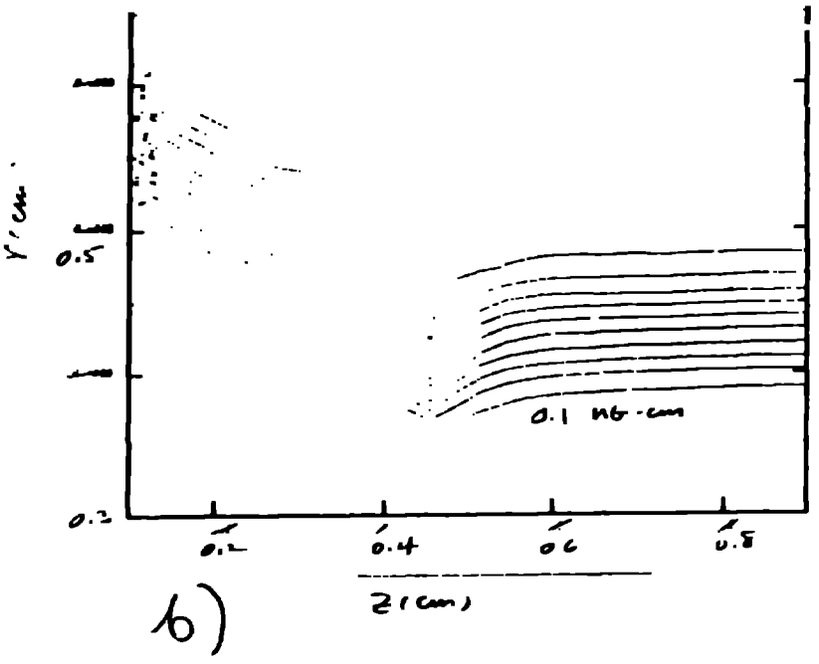

b)

Fig. 4

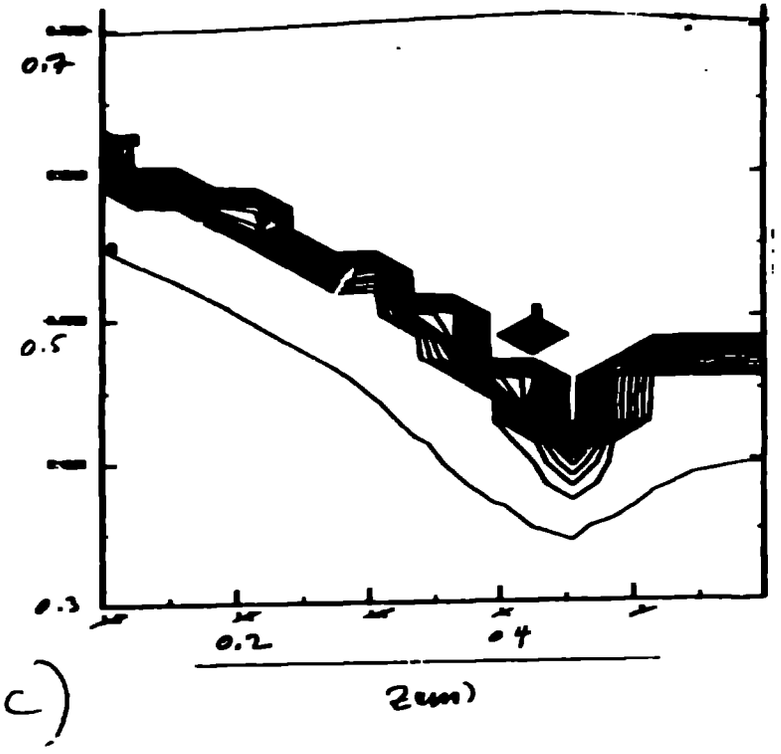

c)

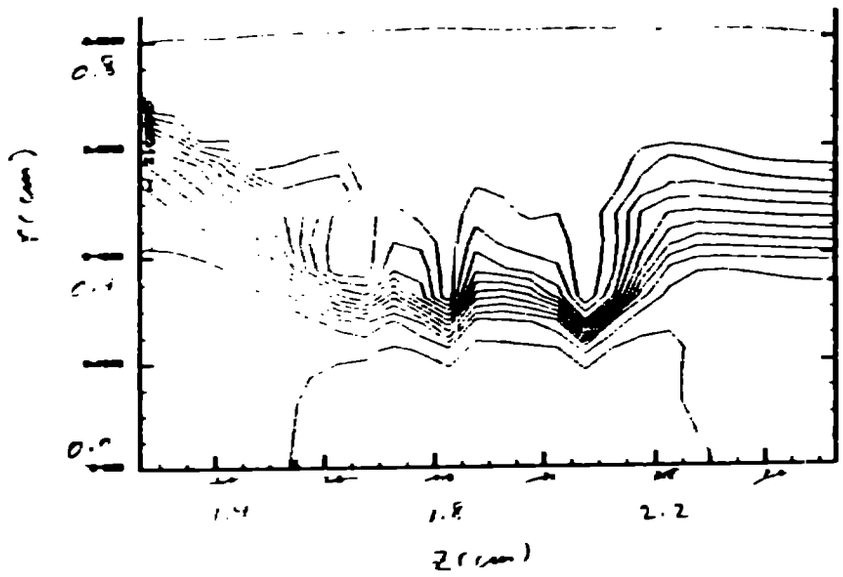

a)

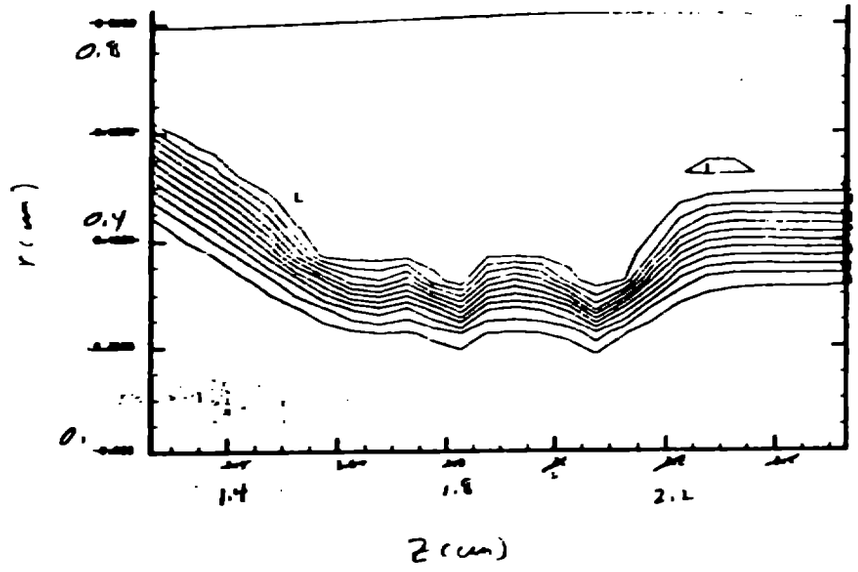

b)

Fig. 5

bowers fig 6

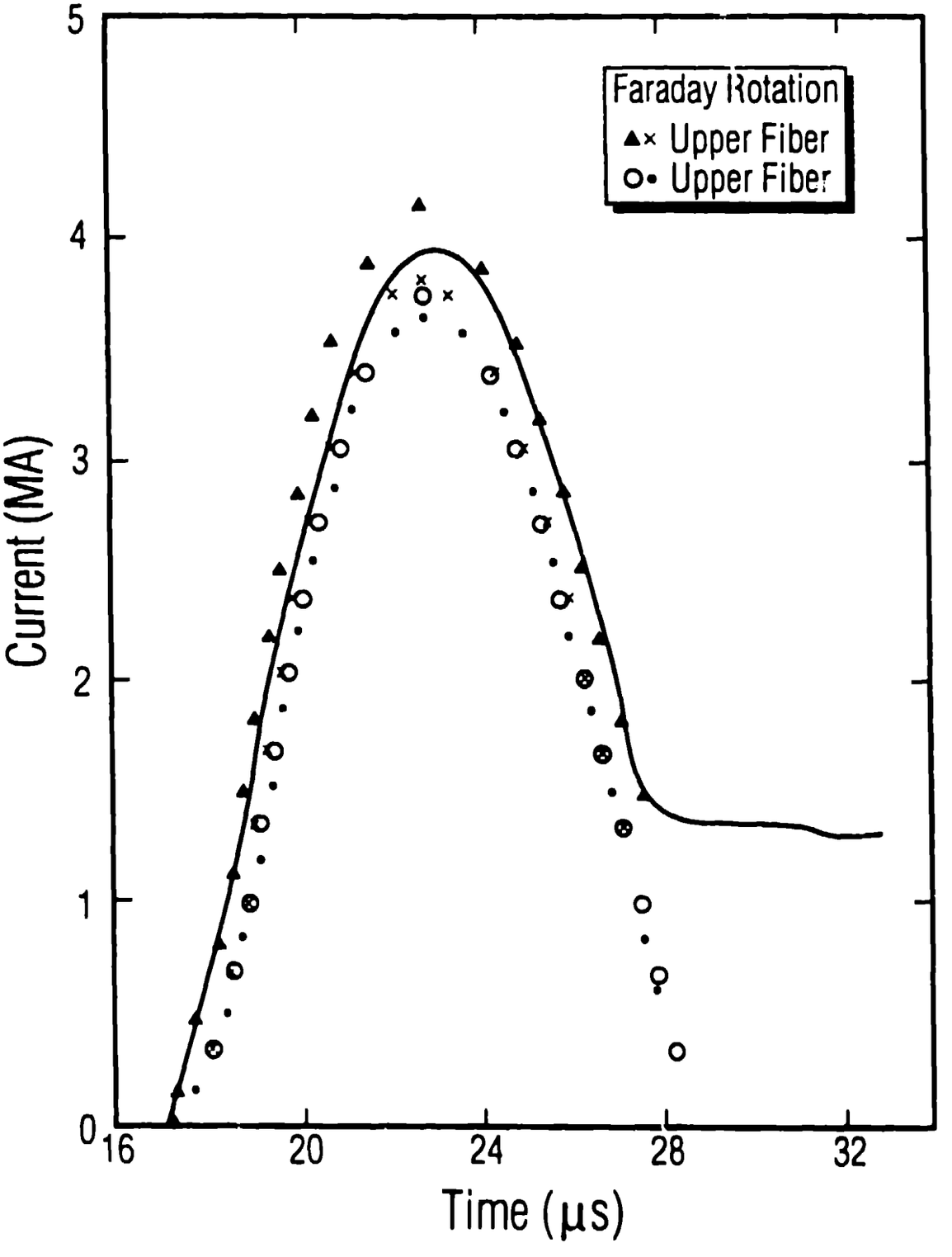

Fig. 6

Fig. 7

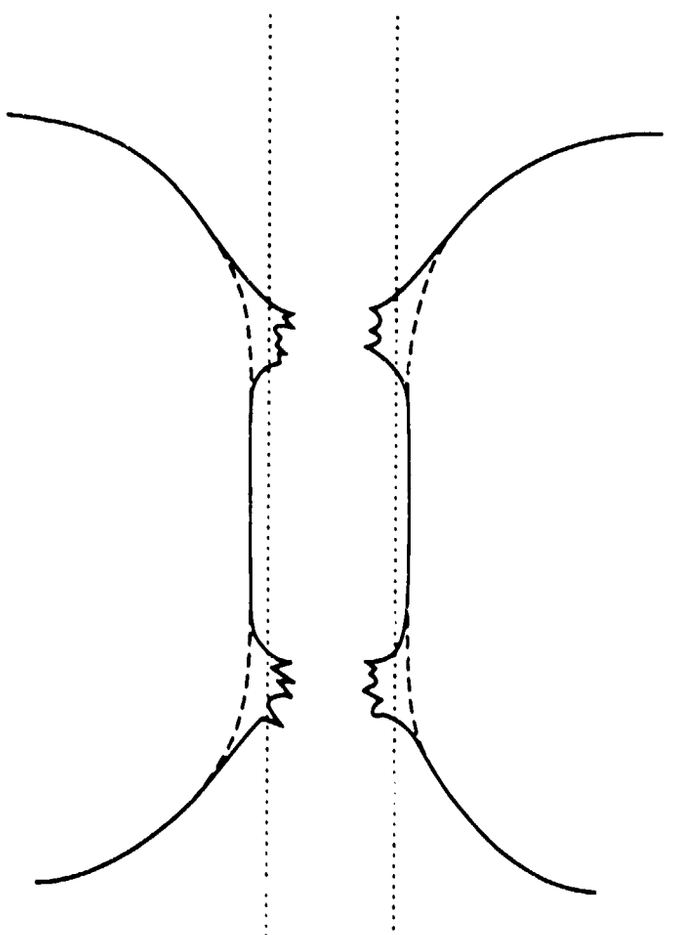

Fig 8

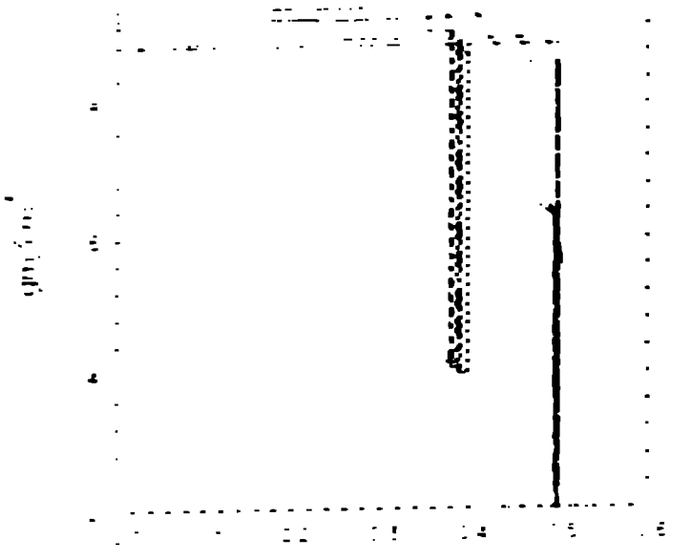

a)

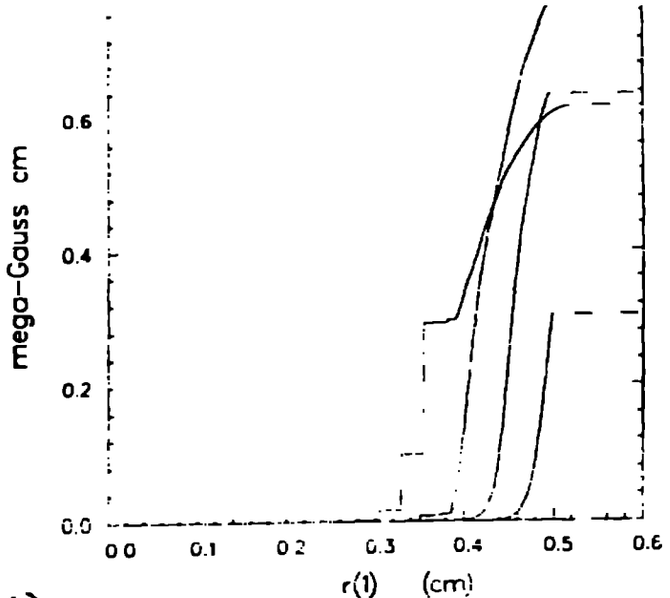
mega-Gauss cm
0.6
0.4
0.2
0.0
0.0
0.1
0.2
0.3
0.4
0.5
0.6
r(1) (cm)

b)

Fig. 9

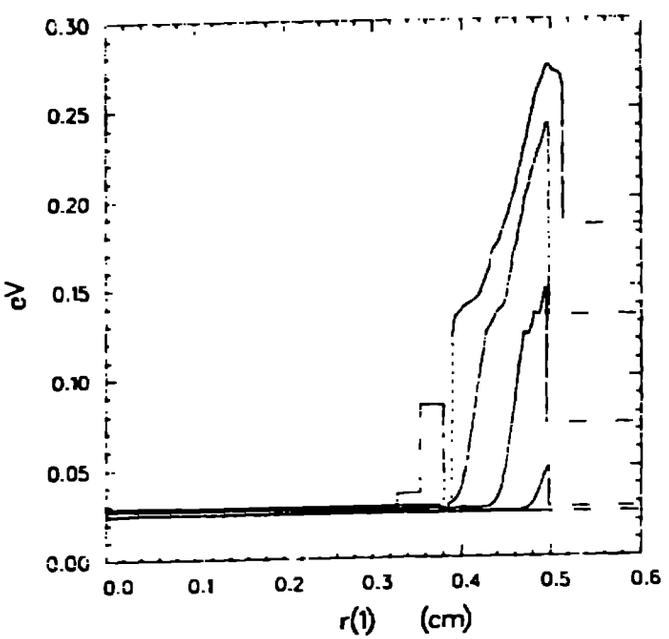
0.30
0.25
0.20
0.15
0.10
0.05
0.00
eV
0.0
0.1
0.2
0.3
0.4
0.5
0.6
r(1) (cm)

c)